AIAA JOURNAL
Vol. 41, No. 2, February 2003

Structural Analysis of Pneumatic Envelopes: Variational Formulation and Optimization-Based Solution Process

Frank E. Baginski*
George Washington University, Washington, D.C. 20052
and
Willi W. Schur†
New Mexico State University, Wallops Island, Virginia 23337

Large super-light structural systems that for functional reasons require large surfaces are composed at least in part of structural membranes. The underconstrained nature of such structural membranes poses analytical challenges, but also provides design opportunities that are not commonly found in other structural systems that require the arsenal of solid-mechanics analytical tools for the assessment of design validity and performance. Overcoming some of the challenges that are posed by the underconstrained nature of such systems is an important ingredient in the development process for gossamer spacecraft. Our approach is a variational formulation of the analytical problem in conjunction with optimization techniques in the solution process. The optimization-based solution process avoids convergence problems that are encountered in the implicit solution process of finite element formulations of these underconstrained structures. To illustrate our approach, we carry out a structural analysis of a pumpkin balloon. Our formulation incorporates wrinkling of the balloon film and structural lack of fit between the skin and the tendon in the unloaded, that is, unstrained, structure. Our results on pumpkin balloons suggest the possibility of similar success if our methods are applied to other pneumatic envelopes.

Nomenclature

$\mathcal{E}_f$	=	gravitational potential energy of the film
$\mathcal{E}_P$	=	hydrostatic pressure potential energy
$\mathcal{E}_T$	=	total energy of the balloon system
$\mathcal{E}_t$	=	gravitational potential energy of the load tendons
$\mathcal{E}_{\mathrm{top}}$	=	gravitational potential energy of the top fitting
G_F	=	flat unstrained reference configuration (natural state) of the pumpkin gore
$\mathcal{G}_F$	=	ideal doubly curved pumpkin gore
n_g	=	number of gores in a complete shape
r_B	=	bulge radius of ideal pumpkin gore
$\mathcal{S}$	=	complete balloon shape
S_f	=	strain energy of balloon film
S_t	=	strain energy of the load tendons
T	=	triangle in a discretization of G_F
$\mathcal{T}$	=	triangle in a discretization of $\mathcal{G}_F$
$\mathcal{V}$	=	volume of balloon $\mathcal{S}$
ϵ_t	=	load tendon slackness parameter
ω_0	=	target volume for an energy minimizing shape when a volume constraint is imposed

I. Introduction

THERE is a desire in the scientific community to have large-scale, long-duration, high-altitude platforms, which have a load-carrying capacity of current zero-pressure balloons. At mid-latitudes zero-pressure balloons are only suitable for short-duration flights. Current long-duration balloons are spherical superpressure designs with a load-carrying capacity that is about 70 times less than that of current zero-pressure balloons. In response to requests by the scientific community, NASA's scientific balloon program embarked on the development of a high-altitude platform that can meet the new needs of that community. This effort led to considering a balloon design that has been discussed since the 1970s but that has only been subjected to analytical treatment since 1998. Various researchers have referred to this design as the pumpkin-shaped balloon (see Fig. 1). The pumpkin design is a significant departure from the zero-pressure balloon that has been the workhorse for NASA's large scientific balloon program since the 1970s. For this reason it is necessary to develop new tools for the analysis of this new class of shapes. The pumpkin balloon involves a totally different geometry for the balloon shape (as compared to past balloon designs) and a structural lack of fit between the film and load tendons, which enables the pumpkin balloon to meet the requirements for a long-duration balloon platform. The zero-pressure, superpressure, and pumpkin balloon designs are discussed further in Sec. II.

Smalley[1] performed some tests on small-scale pumpkin balloons that relied on the elastic properties of the tendons and skin only. He demonstrated improved performance in a qualitative manner only, using very stiff tendons and relatively compliant skin. The French space agency Centre National d'Etudes Spatiales performed some tests on small-scale pumpkin balloons in the late 1970s.[2] In either case, lack of scalable quantitative assessment appears to have prevented more serious consideration of service size pumpkin balloons. In 1998, Yajima[3] experimented with small-scale pumpkin type balloons in which he provided enough skin to allow circular bulging of the unstressed skin between the tendons. He shortened the tendons relative to the gore seams to achieve near circular bulging of the gores from tendon to tendon in the loaded configuration, but no quantitative assessment was provided. The second author[4] pursued the same idea by analytical means. A parametric study of a large number of designs explored those design aspects that lead to the lowest peak stresses in the skin. The results of Ref. 4 demonstrated that the film strength requirement diminished with increasing tendon stiffness. (We include similar parametric studies that demonstrate this as well.) It was easy to deduce that foreshortening of the tendon can substitute for tendon stiffness.[4]

The pumpkin balloon design option, even when limited to a particular mission scenario, is not a single design, but rather it is a large class of design shapes in which material options and fabrication parameters can be chosen to arrive at an efficacious design.

Received 8 November 2001; presented as Paper 2002-1461 at the AIAA 3rd Gossamer Spacecraft Forum, Denver, CO, 22–25 April 2002; revision received 7 October 2002; accepted for publication 22 October 2002.

*Professor of Mathematics, Department of Mathematics; baginski@gwu.edu. Senior Member AIAA.

†Research Engineer, Physical Sciences Laboratory, Field Engineering Group: NASA-GSFC-WFF; willi.w.schur.1@gsfc.nasa.gov. Member AIAA.

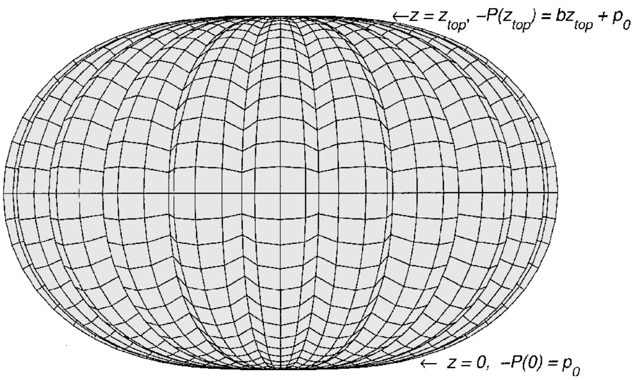

Fig. 1 Pumpkin-shaped balloon.

The basic idea is a design in which fabrication parameters and the matching of material properties of the pneumatic envelope and of its reinforcing tendons are chosen so as to control the load paths, rather than fixing a design without forethought and then accepting stress distributions in the structure as a natural outcome. Other than end fittings, the structural system of the pumpkin balloon comprises the skin, which is also the gas barrier, and the load tendons. The skin carries the pressure load in the hoop-wise direction over a small radius arc to the tendons, and it can also carry some load in the meridional direction. The load tendons are one-dimensional structural elements that provide the bulk of the global pressure confining strength. In a design in which the division of load-carrying functions is complete, the film does not participate in meridional load transfer.

In general, using an implicit solver for determining the load response of pneumatic envelopes is hampered by severe difficulties as a result of the underconstrained nature of the structural system. In performing the analyses in Ref. 4, very small artificial bending stiffness was introduced to enable convergence. Two analyses with artificial bending stiffness differing by nearly a decade were compared to ensure that the membrane solution was not unduly affected by this artifice. The addition of the tension field feature and the initial unstrained wrinkled state further worsen the convergence performance of these analyses. The tension field feature, which is introduced via a nonlinear material model is of particular concern because in the transition zone from membrane to tension field behavior toggling between element states is likely to ensue because truncated response function series can, in general, not mimic vastly different responses within the same element. To avoid toggling, which is a serious impediment to convergence, it is necessary to choose reduced integration point elements, which have the inherent problem of hourglassing. Experimentation with hourglass control was necessary to complete the study. In the present work we triangulate the balloon surface, utilizing a linear isotropic stress-strain relation with a constant strain model. All integrals over the faceted balloon surface are evaluated exactly in terms of the nodal coordinates of the triangles. The gradient of the total balloon energy is computed analytically, aiding convergence of our method. No convergence problems were encountered in the numerical solutions that are presented here. This paper introduces a different analytical approach to the analysis of pneumatic envelopes in general and pumpkin balloons specifically. This type of approach has been applied successfully to the analysis of strained zero-pressure natural shape balloons by the first author and his collaborators.[5–7]

In the present work we consider conditions where the pumpkin balloon is fully deployed. We expect wrinkling to occur, but we do not expect large-scale folds of excess film. A. C. Pipkin's method of energy relaxation methods to model membrane wrinkling[8] was adapted to balloon applications by Collier.[7] The energy relaxation approach fits naturally into the variational formulation and optimization-based solution process and was applied to spool-like and ascent configurations of large scientific balloons in Ref. 5. The previous work[5] assumed there was no slackness in the load tendons. In this paper we modify the model presented in Ref. 5 so that it can accommodate the pumpkin balloon, including a doubly curved gore design, and a structural lack of fit between the tendon and gore.

We formulate a variational principle for the energy of the balloon system and use a standard constrained minimization scheme to determine a solution of a rather difficult nonlinear membrane mechanics problem. We demonstrate that such degenerate material response as tension field response, and excess unstrained material in the unloaded configuration and the concomitant structural lack of fit, can be modeled in a natural way with this formulation by using energy relaxation.

II. Pumpkin Design Shape

Before describing the pumpkin design, we first discuss the so-called natural shape, a design that is obtained from equilibrium considerations alone by requiring that the global confinement of the gas bubble and the carrying of the structural weight of the system be accomplished by a meridional force system. For the shape-finding problem hoop-wise confinement stresses are assumed to be nonexistent in the natural shape. When the differential pressure at the base of the balloon is zero, we refer to the corresponding design as a zero-pressure natural shape balloon. If the differential pressure at the base is greater than zero, we refer to the corresponding design as a superpressure natural shape balloon. In the designs that we consider, the natural shape is determined for a significant internal overpressure that dominates the buoyant pressure component. This is typical of the so-called superpressure balloons, which are capable of float-altitude keeping at midlatitudes without the need of ballasting over a diurnal cycle.

We will consider two types of gore shapes in this paper. One gore shape is obtained by spanning the unstrained gore exactly between two adjacent tendon trajectories that follow the natural shape (see Ref. 9 for more on the natural shape). In this configuration the gore forms a developable surface. The other gore shape generates the pumpkin balloon and is obtained by prescribing outward bulging of the unstrained gore between adjacent tendon trajectories. The bulging surface that spans adjacent tendons has positive Gaussian curvature in the pumpkin balloon. To achieve this general shape with an unstrained flat sheet, the sheet must be allowed to wrinkle. In Sec. V.C these two gore shapes are each paired with tendons of varying amounts of slackness (negative slackness corresponds to tendon shortening). The pumpkin design considered in Sec. V.C was the same as the one used for a NASA Ultra-Long Duration Balloon (ULDB) that was flown in 2001. We also consider several other parametric studies related to the pumpkin balloon, including variations of the bulge radius and number of gores.

Gore designs that use developable surfaces are typical of current so-called zero-pressure natural shape balloons. Generally, these zero-pressure balloons have load tendons, leading to strained shapes with nonzero hoop stresses and violating the underlying assumptions of the shape-finding process for the so-called natural shape. By contrast, designs with shortened tendons, and in particular those that in addition have gores that are designed with initial positive Gaussian curvature, lead to a strained shape that might at least in an approximate sense satisfy the design shape assumptions.

To demonstrate parameter sensitivity in the pumpkin balloon problem, we carried out a number of numerical studies. In one case we fix the bulge radius and vary the number of gores n_g (see Parametric Study A in Sec. V.A). We consider balloons with 220, 290, and 400 gores. If the bulge radius is too small for a given n_g, there might be insufficient material to span the tendons, and a pumpkin balloon design might not exist. In Parametric Study B in Sec. V.B, we fix the number of gores and vary the bulge radius r_B. We consider pumpkin balloons with 290 gores, and $r_B = 0.66$, 0.78, 0.90, and 1.20. In Parametric Study C in Sec. V.C, we fix the number of gores and bulge radius and vary a parameter (ϵ_t) that controls tendon slackness (that is, tendon/film mismatch).

Theoretically, the more efficient pumpkin gore design is obtained with a constant bulge radius because the skin is nearly equally stressed over the entire gore length. However, in the presence of manufacturing imperfections a local gore-width shortfall, although harmless near the equator, can produce a disastrous stress raiser near the gore ends. Therefore, the initial design with constant bulge radius was modified by an addition of some constant gore width over the entire gore length for NASA's ULDB (used in Parametric

Table 1 Default design parameters and related constants for ϵ_t studies

Description	Variable	Value
Weight of top fitting	w_{top}	831 N
Cap weight density	w_c	0.18387 N/m^2
Film weight density	w_f	0.3440 N/m^2
Young's modulus	E	404.2 MPa
Poisson ratio	ν	0.825
Film thickness	h	38.1 μm
Tendon weight density	w_t	0.094 N/m
Tendon stiffness	K_t	0.651 MN
Payload	L_{bot}	20,393 N
Design specific buoyancy	b	0.0763 N/m^3
Number of gores	n_g	290
Cap length	l_c	49.45 m
Constant pressure	p_0	135 Pa
Target volume	ω_0	0.5215 Mm^3
Length of curved gore edge	L_d	152.034 m
Gore length (center gore)	L_c	152.027 m
Length of pumpkin generator	L_p	150.023 m
Length of tendon (before tensioning)	L_t	147.573 m
Length of tendon (after tensioning)	$\hat{L}_t$	148.744 m

Study C in Sec. V.C; see Table 1 for design parameters). The latter provision hardly changes the bulge radius near the equator, but it reduces the bulge radius progressively as the gore station approaches the vertical axis of the balloon.

To demonstrate the effectiveness of a pumpkin shape design, we carried out stress analyses on six balloon designs in Parametric Study C. Three designs use a gore that in its unstrained state forms a developable surface spanning two adjacent tendon trajectories, and three designs in which sufficient gore-width and gore-length are supplied to allow circular arc bulging between the tendons. The latter, we refer to as pumpkin-shape balloons and the former as standard natural-shape balloons. We will consider the following scenarios: (C1) a standard natural-shape balloon with 2.99% tendon slackness; (C2) a standard natural-shape balloon with tendon length matching the gore seam length; (C3) a standard natural-shape balloon with 2.22% shortening of the tendon relative to the gore seam; (C4) a pumpkin-shape balloon with 2.99% tendon slackness; (C5) a pumpkin-shape balloon with tendon length matching the gore seam length; and (C6) a pumpkin-shape balloon with 2.22% shortening of the tendon relative to the gore seam. In Parametric Studies A and B tendons were shortened by 2.22% in all cases.

A baseline superpressure natural-shape balloon profile based on a volume of 521,500 m^3 was generated for comparison with the pumpkin balloon. In Parametric Studies A and B the specific buoyancy b, r_B, and the payload are slightly higher. For design purposes we assumed that a 0.8-mil polyethylene cap covered the top portion of the balloon. However, in our stress analysis we assumed that the balloon skin was a single layer of 1.5-mil polyethylene.

Next, we define an ideal doubly curved pumpkin gore. The pumpkin gore can be parameterized as a tubular surface (see Ref. 10, p. 89). Let $\boldsymbol{\alpha}(s) = [R_p(s), 0, Z_p(s)]$ for $0 < s < L_p$ be a generating curve for the tubular surface, where s is arc length [i.e., $|\boldsymbol{\alpha}'(s)| = 1$]. When n_g is large, $\boldsymbol{\alpha}$ roughly follows the shape of the generating curve for a natural shape. For convenience, we assume $\boldsymbol{\alpha}$ lies in the xz plane. The ideal pumpkin gore is a subset of a tubular surface defined by the following map:

$$\boldsymbol{x}(s, v) = \boldsymbol{\alpha}(s) + r_B[\boldsymbol{j}\sin v - \boldsymbol{b}(s)\cos v] \tag{1}$$

where $-v_{r_B}(s) < v < v_{r_B}(s)$, $0 < s < L_p$, $\boldsymbol{b}(s)$ is the inward normal to $\boldsymbol{\alpha}(s)$, and $v_{r_B}(s)$ is determined so that

$$y\big(s, v_{r_B}(s)\big) = \tan(\pi/n_g)x\big(s, v_{r_B}(s)\big)$$

where $x(s, v) = \boldsymbol{x}(s, v) \cdot \boldsymbol{i}$ and $y(s, v) = \boldsymbol{x}(s, v) \cdot \boldsymbol{j}$ (Fig. 2). Because the gore is symmetric, the lower bound for v is $-v_{r_B}(s)$. A unit tangent to $\boldsymbol{\alpha}(s)$ is $\boldsymbol{t}(s) = \boldsymbol{\alpha}'(s)$ and $\boldsymbol{t} \times \boldsymbol{b} = \boldsymbol{j} = (0, 1, 0)$. It can be shown that

$$\boldsymbol{a}_1(s, v) = \frac{\partial \boldsymbol{x}}{\partial s}(s, v) = \boldsymbol{t}(s), \qquad -r_B(s) < v < r_B(s)$$

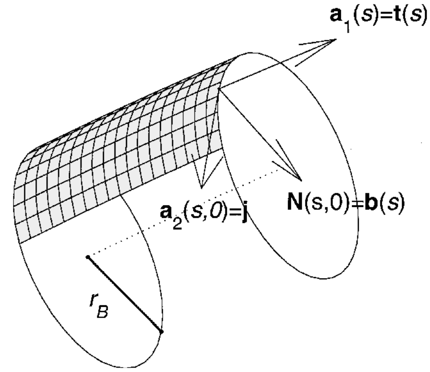

Fig. 2 Subset of a tubular surface defining a pumpkin gore.

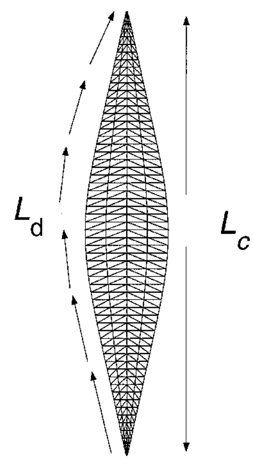

Fig. 3 Flat reference configuration (gore pattern).

and that

$$\boldsymbol{a}_2(s, 0) = \frac{\partial \boldsymbol{x}}{\partial v}(s, 0) \Bigg/ \left|\frac{\partial \boldsymbol{x}}{\partial v}(s, 0)\right| = \boldsymbol{j}$$

(Fig. 2). We define the ideal three-dimensional pumpkin gore to be the set

$$\mathcal{G}_F = \{(x, y, z) = \boldsymbol{x}(s, v),\ (s, v) \in \Omega_F\} \tag{2}$$

where the parameter space Ω_F is given by

$$\Omega_F = \big\{(s, v) \mid 0 < s < L_p, -v_{r_B}(s) < v < v_{r_B}(s)\big\} \tag{3}$$

Corresponding to $\mathcal{G}_F$, we define the flat reference configuration by

$$G_F = \{(Y, Z) \mid Y = r_B v,\ Z = Z_c(s),\ (s, v) \in \Omega_F\} \tag{4}$$

where $Z_c(s)$ is measured down the center of the gore [i.e., $Z_c(L_p) = L_c$]. The gore seam length is denoted by L_d. The tendon length is denoted by L_t (Fig. 3).

Remark: As mentioned earlier, the nominal gore design of fixed bulge radius was modified by a small constant width addition for the ϵ_t studies. This in fact causes the effective bulge radius to vary along the gore length and to become increasingly smaller toward the gore ends. We can take these alterations into account by appropriately modifying G_F. The flat reference configuration G_F used in our analysis of pumpkin shapes in Parametric Study C is the gore pattern that was used in the construction of an ultra-long-duration pumpkin balloon flown by NASA (a 521,500 m^3 pumpkin balloon with bulge radius $r_B = 0.835$ m). For the r_B and n_g studies additional width was not added.

Figure 3 contains a representation of the discretization of G_F. The reference configuration displayed in Fig. 3 has been rescaled to illustrate the grid. We will assume that the complete pumpkin gore is located symmetrically about the $y = 0$ plane in $\mathbb{R}^3$. By symmetry, we need to model only the right half-gore. Let $\mathcal{G}_F^0$ denote initial configuration of the pumpkin gore in $\mathbb{R}^3$. Because $\mathcal{G}_F^0$ and the strained pumpkin gore are deformations of a flat gore G_F into a shape that has positive Gauss curvature, they are necessarily strained and possibly wrinkled in certain regions.

Consistent with the design criteria for a pumpkin balloon, we assume that the load tendon is 2.22% shorter than the length of the gore edge L_d (after tensioning). This means that each tendon segment identified with a gore edge segment in G_F^0 must be stretched initially by 2.22%. Thus, we are able to define the initial geometry of the balloon film and tendon, including the structural lack of fit as described by Schur.[4] We emphasize the initial pumpkin configuration (with tendon/film mismatch) is prestrained and need not be in equilibrium. $\mathcal{G}_F^0$ is merely used as the starting shape, which is evolved to the equilibrium shape. In our parametric studies involving ϵ_t, the initial complete shape $\mathcal{S}^0$ is taken to be a sphere of circumference $2L_d$ with load tendons (initially of length L_t) strained by 2.22% to match the length of a meridian. For the r_B and n_g parametric studies we use $\mathcal{G}_F$ as the initial starting configuration and G_F as the natural unstrained shape, but additional material is not added to the gore width and length.

III. Mathematical Model

The total potential energy of a balloon configuration $\mathcal{E}_T$ is the sum of six terms:

$$\mathcal{E}_T = \mathcal{E}_P + \mathcal{E}_f + \mathcal{E}_t + \mathcal{E}_{\text{top}} + S_t + S_f \tag{5}$$

where $\mathcal{E}_{\text{top}} = w_{\text{top}} z_{\text{top}}$ is the energy of the top fitting. In the following it will be useful at times to consider $\mathcal{S}$ as a faceted surface. In this case $\mathcal{T}$ will denote a typical facet in $\mathcal{S}$, corresponding to $T \in G_F$.

A. Hydrostatic Pressure Potential

We follow the conventions for hydrostatic differential pressure P presented in Ref. 9, p. II-7, where $-P(z) > 0$ means that the inside of the balloon is pushing outward at height z above the base of the balloon. For a superpressure balloon $-P(z) = bz + p_0$, where b is the specific buoyancy, $p_0 > 0$, and $p_0 \gg bz_{\text{top}}$. For example, the variation in differential pressure caused by a specific buoyancy of $b = 0.0763$ N/m^3 leads to a differential pressure variation that is linear in z with $-P(0) = 135$ Pa and $-P(z_{\text{top}}) = 142$ Pa. In our choice of coordinates, we generally assume that the base of the balloon is fixed and corresponds to $z = 0$ (see Fig. 1). The potential for hydrostatic pressure $P(z)$ is

$$\mathcal{E}_P = \int_{\mathcal{V}} P(z)\,\mathrm{d}V = -\int_{\mathcal{V}} (bz + p_0)\,\mathrm{d}V \tag{6}$$

where $\mathcal{V}$ is the region occupied by the gas bubble. Using the divergence theorem and the symmetries of $\mathcal{S}$, Eq. (6) can be written as

$$\mathcal{E}_P = -n_g \int_{\Omega_F} \left(\frac{1}{2}bz^2 + p_0 z\right)\boldsymbol{k} \cdot \mathrm{d}\boldsymbol{S} \tag{7}$$

where $\mathrm{d}\boldsymbol{S} = \boldsymbol{N}\,\mathrm{d}S$, $\boldsymbol{N}$ is the unit outward normal to $\mathcal{S}$, and $\mathrm{d}S$ is the surface area measure on $\mathcal{S}$.

In a closed system where the volume is fixed and p_0 is unknown, we begin the evolution of an equilibrium shape with $-P(z) = bz$. After calculating a solution, the Lagrange multiplier associated with the volume constraint yields the appropriate constant pressure term p_0 that is needed for equilibrium (see Ref. 7, p. 35).

B. Gravitational Potential Energy

The gravitational potential energy from the weight of the balloon film is

$$\mathcal{E}_f = \int_{\mathcal{S}} w_f z\,\mathrm{d}A \tag{8}$$

where the film weight density is w_f and $\mathrm{d}A$ is area measure in the natural state. Cap weight can be incorporated by modifying w_f appropriately.

Let Γ denote the right edge of a gore. The image of Γ in the deformed configuration is a curve parametrized by $\boldsymbol{\tau}(s) \in \mathbb{R}^3$, where s is arc length measured along the edge of the gore in its natural state. A load tendon runs along the seam of the balloon from top endcap to bottom endcap. The load tendon lies along the curve parametrized by $\boldsymbol{\tau}$. The gravitational potential energy caused by load tendon weight is

$$\mathcal{E}_t = n_g w_t \int_0^{L_t} \boldsymbol{\tau}(s) \cdot \boldsymbol{k}\,\mathrm{d}s \tag{9}$$

where w_t is the load tape weight density.

C. Balloon Film Strain Energy

We will use the film strain energy measure as defined in Ref. 5. Details are provided here for the convenience of the reader. In Chapter 7, Sec. 1, of Ref. 11, Ciarlet derives the two-dimensional Koiter equations for a nonlinear elastic shell. Using this formulation and ignoring the bending or flexural energy because the thickness is so small, we can express the resulting film strain energy S_f in the form

$$S_f = n_g \int_{\Omega_F} W_f\,\mathrm{d}A \tag{10}$$

where

$$W_f = \tfrac{1}{2}\boldsymbol{n} : \boldsymbol{\gamma} \tag{11}$$

is the strain energy density function of the balloon film and Ω_F denotes the parameter space for the flat reference configuration. See Ref. 5 for further details as well as the discretization used in numerical calculations. In Eq. (11) $\boldsymbol{n}$ represents the second Piola–Kirchhoff stress tensor, $\boldsymbol{\gamma}$ represents the Cauchy–Green strain tensor, and ":" is the tensor inner product. The contravariant components of $\boldsymbol{n}$ are denoted by $n^{\alpha\beta}$, the covariant components of $\boldsymbol{\gamma}$ are denoted by $\gamma_{\alpha\beta}$, and $\boldsymbol{n} : \boldsymbol{\gamma} = n^{\alpha}_{\beta}\gamma^{\beta}_{\alpha}$. Assuming a linear elastic isotropic material, we have

$$n^{\alpha\beta} = E^{\alpha\beta\lambda\mu}\gamma_{\lambda\mu} \tag{12}$$

where $E^{\alpha\beta\lambda\mu}$ is the tensor of elastic moduli, that is,

$$E^{\alpha\beta\lambda\mu} = \frac{hE}{2(1+\nu)}\left[a^{\alpha\lambda}a^{\beta\mu} + a^{\alpha\mu}a^{\beta\lambda} + \frac{2\nu}{1-\nu}a^{\alpha\beta}a^{\lambda\mu}\right] \tag{13}$$

E is Young's modulus, ν is Poisson's ratio, h is the shell thickness, and

$$[a_{\alpha\beta}] = \begin{bmatrix} 1 & 0 \\ 0 & 1 \end{bmatrix}$$

is the first fundamental form of the flat reference configuration.

Ultimately, we want to express the strain energy as a function of the nodes of the triangular facets in $\mathcal{S}$. We first define all of the geometric and physical quantities for a typical facet. Let v_0, v_1, v_2 be the vertices of $\mathcal{T}$ and V_0, V_1, V_2 be the vertices of T. A constant strain model can be defined in the following way: Let R be the linear map that takes a standard triangle with sides $\boldsymbol{i} = (1, 0)$, $\boldsymbol{j} = (0, 1)$ to $T \in G_F$, and let D be the linear map that takes the standard triangle to $\mathcal{T} \in \mathcal{G}_F$. The mappings R and D can be represented by 2×2 and 3×2 matrices, respectively.[5] The mapping $p \in T \to q \in \mathcal{T}$ is given by $q = DR^{-1}p$ is linear, and so the deformation gradient on T is

$$\boldsymbol{F} = \frac{\partial q}{\partial p} = DR^{-1}$$

The Cauchy strain is $\boldsymbol{C} = \boldsymbol{F}^T\boldsymbol{F}$, and the Cauchy–Green strain (γ) is $\boldsymbol{G} = \frac{1}{2}(\boldsymbol{C} - \boldsymbol{I})$. Assuming an isotropic film and the linear stress-strain relation in Eq. (12), the second Piola–Kirchhoff stress can be written as

$$\boldsymbol{S} = \lambda[\boldsymbol{G} + \nu\,\mathrm{Cof}(\boldsymbol{G})^T] \tag{14}$$

where $\lambda = Eh/(1-\nu^2)$ and the 2×2 cofactor matrix is

$$\mathrm{Cof}\left(\begin{bmatrix} a_{11} & a_{12} \\ a_{21} & a_{22}\end{bmatrix}\right) = \begin{bmatrix} a_{22} & -a_{12} \\ -a_{21} & a_{11}\end{bmatrix}$$

$\boldsymbol{G}$ and $\boldsymbol{S}$ are symmetric, and by the spectral representation theorem, we have

$$\boldsymbol{G} = \delta_1 \boldsymbol{n}_1 \otimes \boldsymbol{n}_1 + \delta_2 \boldsymbol{n}_2 \otimes \boldsymbol{n}_2 \tag{15}$$

$$\boldsymbol{S} = \mu_1 \boldsymbol{n}_1 \otimes \boldsymbol{n}_1 + \mu_2 \boldsymbol{n}_2 \otimes \boldsymbol{n}_2 \tag{16}$$

where $\boldsymbol{n}_1$ and $\boldsymbol{n}_2$ are orthonormal vectors. The eigenvalues of $\boldsymbol{S}$ (denoted by μ_1 and μ_2) are the principal stress resultants, and the eigenvalues of $\boldsymbol{G}$ (denoted by δ_1 and δ_2) are principal strains. Because we have assumed a linear and isotropic relationship between the stress and strain, $\boldsymbol{S}$ and $\boldsymbol{G}$ have the same principle axes. The film strain energy density on triangle T is given by

$$W_f(T) = \tfrac{1}{2}\boldsymbol{S} : \boldsymbol{G} \tag{17}$$

The energy density in Eq. (17) can lead to states where μ_1 or μ_2 are negative, corresponding to a compression. However, the balloon film cannot support such a compression and will actually fold or wrinkle instead. To tackle the problem of negative compressive stresses in the solution, we follow the methods introduced by Pipkin.[8] In Pipkin's approach a membrane M is decomposed into three distinct regions: S, slack region (where the Cauchy–Green strains are both negative, i.e., $\delta_1 < 0$, $\delta_2 < 0$); T, tense region (where both principal stress resultants are positive, i.e., $\mu_1 > 0$, $\mu_2 > 0$); and U, wrinkled region ($\mathsf{U} = \mathsf{M}\backslash\mathsf{S} \cup \mathsf{T}$). We apply the preceding classification scheme to each $\mathcal{T} \in \mathcal{G}_F$.

On S the strain energy is assumed to be zero, and on T the relaxed strain energy density is exactly the same as the standard strain energy density. On the region U we use a modified Cauchy–Green strain $\boldsymbol{G}^*$ that is defined as follows. If $\boldsymbol{G}$ is the usual Cauchy–Green strain, then

$$\boldsymbol{G}^* = \boldsymbol{G} + \beta^2 \boldsymbol{n} \otimes \boldsymbol{n} \tag{18}$$

where $\boldsymbol{n}$ is an unknown principal stress direction based on $\boldsymbol{G}^*$. Pipkin refers to $-\beta^2 \boldsymbol{n}\otimes\boldsymbol{n}$ as the wrinkling strain and $\boldsymbol{G}^*$ as the elastic strain. The elastic strain is thought to represent the straining in an averaged wrinkled surface and leads to uniaxial stress on U in the form

$$\boldsymbol{S}^* = \mu \boldsymbol{t} \otimes \boldsymbol{t} \tag{19}$$

where $\mu > 0$ and $\boldsymbol{t}$ is a unit vector orthogonal to $\boldsymbol{n}$. For our exposition we assume that $\boldsymbol{t}$ is the tensile direction and $\boldsymbol{n}$ is a unit vector orthogonal to $\boldsymbol{t}$. The parameter β^2 and $\boldsymbol{n}$ are chosen in such a way that the following conditions are satisfied:

$$\boldsymbol{n} \cdot \boldsymbol{S}^* \boldsymbol{n} = 0 \tag{20}$$

$$\boldsymbol{n} \cdot \boldsymbol{S}^* \boldsymbol{t} = 0 \tag{21}$$

For an isotropic material $\boldsymbol{S}^*$ can be written in the form

$$\boldsymbol{S}^* = \boldsymbol{S} + \lambda\beta^2[\boldsymbol{n}\otimes\boldsymbol{n} + 2\nu\,\mathrm{Cof}(\boldsymbol{n}\otimes\boldsymbol{n})^T]$$

It follows that for an isotropic material[5]

$$\beta^2 = -(1/\lambda)\boldsymbol{n}\cdot\boldsymbol{S}\boldsymbol{n} \tag{22}$$

If $W_f(\boldsymbol{G})$ is the standard strain energy density function, the relaxed strain energy density is $W_f(\boldsymbol{G}^*)$, where $\boldsymbol{G}^*$ uses β^2 from Eq. (22) and $\boldsymbol{t}$ is the principal direction that corresponds to a positive principal strain. Wrinkling is modeled by replacing the standard energy density W_f by its relaxation W_f^*. Because W_f^* is constant on each T, we have

$$W_f^*(T) = \begin{cases} 0, \quad \delta_1 < 0 \quad \text{and} \quad \delta_2 < 0 \\ \dfrac{1}{2}hE\delta_2^2, \quad \mu_1 \le 0 \quad \text{and} \quad \delta_2 \ge 0 \\ \dfrac{1}{2}hE\delta_1^2, \quad \mu_2 \le 0 \quad \text{and} \quad \delta_1 \ge 0 \\ \dfrac{hE}{2(1-\nu^2)}\left(\delta_1^2 + \delta_2^2 + 2\nu\delta_1\delta_2\right), \quad \mu_1 \ge 0 \quad \text{and} \quad \mu_2 \ge 0 \end{cases} \tag{23}$$

The membrane energy of a wrinkled balloon is given by

$$S_f^* = \int_\Omega W_f^*\,\mathrm{d}A \tag{24}$$

The contribution caused by caps can be modeled by modifying h and E appropriately.

D. Strain Energy of Tendons

Let $\bar{s}$ denote arc length measured along the edge of Γ [i.e., $\mathrm{d}\bar{s}/\mathrm{d}s = |\boldsymbol{\tau}'(s)|$]. We define the strain in the tendon as

$$\epsilon = \tfrac{1}{2}[|\boldsymbol{\tau}'(s)|^2 - 1]$$

We assume that a segment in a load tendon behaves like a linearly elastic string with stiffness constant K_t. The strain energy density of a tendon is denoted by

$$W_t(\epsilon) = \tfrac{1}{2}K_t\epsilon^2$$

The convexification of the strain energy density for the load tendon is given by

$$W_t^*(\epsilon) = \begin{cases} W_t(\epsilon), & \epsilon \ge \epsilon_t \\ 0, & \epsilon < \epsilon_t \end{cases}$$

Load tendon slackness and tendon shortening are controlled by the parameter ϵ_t. If the tendon length matches the gore edge length and there is no slackness in the tendon, then $\epsilon_t = 0$. In Sec. V, tendon slackness of 2.99% in cases C1 and C4 are modeled by setting $\epsilon_t = 0.0299$, whereas tendon shortening of 2.22% in cases C3 and C6 are modeled by setting $\epsilon_t = -0.0222$. The total relaxed strain energy of the load tendons is

$$S_t^* = n_g \int_\Gamma W_t^*(\varepsilon)\,\mathrm{d}s \tag{25}$$

IV. Variational Principle

The discrete form of the total energy of $\mathcal{S}$ with relaxed strain energies is denoted by $\mathcal{E}_T^*(\mathcal{S})$ and is obtained using Eqs. (7–9), (24), and (25) in Eq. (5).

Using the divergence theorem, the volume of the balloon $\mathcal{S}$ can be expressed as

$$\mathcal{V}(\mathcal{S}) = \int_\mathcal{V} 1\,\mathrm{d}V = \int_\mathcal{S} z\boldsymbol{k}\cdot\mathrm{d}\boldsymbol{S} \tag{26}$$

The volume constraint is in the form

$$\mathcal{V}(\mathcal{S}) = \omega_0 \tag{27}$$

where ω_0 is the target volume. We are led to the following variational principle for computing an equilibrium shape:

Problem ⋆

Minimize:

$$\mathcal{E}_T^*(\mathcal{S})$$

For $\mathcal{S} \in \mathcal{C}_{n_g}$,

Subject to:

$$\boldsymbol{G}(\mathcal{S}) = \boldsymbol{0}$$

where the first component of $\boldsymbol{G} = \boldsymbol{0}$ is defined by the equality constraint (27) (when a closed system is modeled) and the remaining components follow from the symmetry condition that the gore seams lie in the plane $y = \pm\tan(\pi/n_g)x$. $\mathcal{C}_{n_g}$ denotes the class of balloon shapes with dihedral symmetry D_{n_g} (see Ref. 5). For a closed system $P(z) = -bz$, and p_0 is obtained from the Lagrange multiplier associated with the volume constraint. When an open system is modeled, we assume $P(0) = -p_0$ is known. In this case the volume constraint is removed from $\boldsymbol{G}$ and the differential pressure is in the form $P(z) = -bz - p_0$. A solution of Problem ⋆ is called an energy-minimizing shape. MATLAB® software (fmincon) is used to solve a discretization of Problem ⋆.

V. Numerical Results

In this section we present results of our parametric studies on pumpkin balloons. Parametric Study A varies n_g, Study B varies r_B, and Study C varies ϵ_t. To demonstrate the effectiveness of the pumpkin design, we include a comparison of a pumpkin balloon with a superpressure natural shape balloon as a part of Study C. In tables and plots we present principal stresses (i.e., $\bar{\sigma}_i^* = \bar{\mu}_i/h$, where h is the thickness and $\bar{\mu}_i$ is a principal stress resultant). The notation $\bar{\sigma}_i = \bar{\sigma}_i(s)$ indicates this value is an average of the principal stress of adjacent triangles in a strip that is located s meters from the bottom of the gore.

A. Parametric Study A with Varying n_g

In Table 2 we fix $r_B = 0.90$ and $\epsilon_t = -0.0222$ and compute pumpkin designs with $n_g = 220$, 290, and 400. We solved Problem ⋆ for each design and recorded the maximum principal stresses. As the number of gores increases, we note from Table 2 that the total weight of the balloon increases. A balloon with 400 gores is about 7% heavier than one with 220 gores. However, the maximum film stress in a balloon with 400 gores is 56% less than the maximum film stress in a balloon with 220 gores. Although it is clear from Table 3 that increasing the number of gores reduces the maximum film stresses, the corresponding 7% weight increase is significant. In addition, there can be manufacturing difficulties with building gores that are very narrow near the ends. In practice, the balloon designer must reach a compromise between factors such as film weight and film strength when choosing a particular design.

B. Parametric Study B with Varying r_B

In Table 4 we fix $n_g = 290$ and $\epsilon_t = -0.0222$ and vary r_B between 0.66 and 1.20. If R^* is the maximum radius of the tendon and n_g is the number of gores, then r_B must be chosen so that

$$r_B \geq R^* \sin(\pi/n_g)$$

Table 2 Parametric Study A: Vary n_g with $r_B = 0.90$, $\epsilon_t = -0.0222$, and $p_0 = 170$

Variable	$n_g = 220$	$n_g = 290$	$n_g = 400$
L_d, m	152.771	153.95	152.77
L_t, m	154.54	156.246	154.54
θ_0	89.14	89.17	89.19
H, m	70.78	71.18	72.07
$d_{\max}$, m	117.48	118.50	120.14
V, m^3	584,992	599,962	625,006
A, m^2	40,387	38,148	37,937
Lift, N	50,906	52,209	54,388
W_{cap}, N	4,239	4,064	3,981
W_t, N	4,380	5,837	8,173
W_{skin}, N	13,893	13,123	13,050

Table 3 Maximum principal stresses in Parametric Study A: Vary n_g with $r_B = 0.90$ and $\epsilon_t = -0.0222$

Stress	$n_g = 220$	$n_g = 290$	$n_g = 400$
Max σ_1, MPa	4.76	1.52	0.00
Max σ_2, MPa	10.15	5.89	4.45

Table 4 Parametric Study B: Vary r_B with $n_g = 290$, $\epsilon_t = -0.0222$, and $p_0 = 170$

Variable	SPNS	$r_B = 0.66$	$r_B = 0.78$	$r_B = 0.90$	$r_B = 1.20$
L_d, m	155.26	157.174	154.87	153.95	155.7
L_t, m	155.26	158.294	156.7	156.24	156.14
$\theta(s=0)$, deg	89.19	89.17	89.17	89.17	89.17
H, m	72.17	72.8	71.7	71.18	70.26
$d_{\max}$, m	119.22	120.77	119.20	118.50	117.45
V, m^3	584,742	627,343	606,839	599,962	593,350
A, m^2	35,153	44,256	39,652	38,148	36,672
Lift, N	50,884	54,591	52,807	52,209	51,633
W_{cap}, N	378	4,267	4,125	4,064	4,018
W_t, N	5,800	5,914	5,857	5,837	5,820
W_{skin}, N	12,092	15,224	13,640	13,124	12,615

Table 5 Maximum principal stresses in Parametric Study B: Vary r_B with $n_g = 290$ and $\epsilon_t = -0.0222$

Stress	B1 $r_B = 0.66$	B2 $r_B = 0.78$	B3 $r_B = 0.90$	B4 $r_B = 1.20$
Max σ_1, MPa	1.89	1.58	1.52	1.68
Max σ_2, MPa	7.53	6.13	5.87	7.29

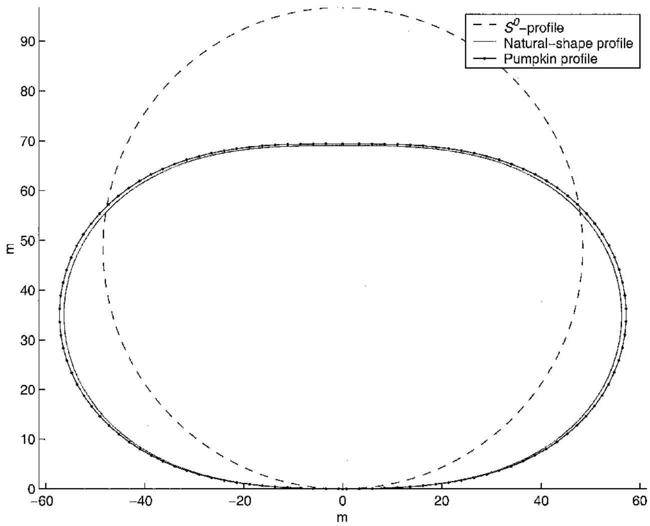

Fig. 4 Balloon profiles: - - -, $\mathcal{S}^0$, sphere of circumference $2L_d$; ——, strained standard natural shape; and -·-, strained pumpkin shape.

For case B we determined the minimum r_B to be about 0.60 m. If smaller values of r_B are used, the corresponding circular arc will not be able to span adjacent load tendons. We solved Problem ⋆ for each design presented in Table 4 and recorded the results. For the cases considered here, we found that the minimum of the maximum principal stresses for cases B1, B2, B3, and B4 occurred in case B3 with $r_B = 0.90$ (Table 5). In the ϵ_t studies the maximum principal stresses are smaller, but the buoyancy and p_0 are lower, and extra length and width were added to the gores.

C. Parametric Study C with Varying ϵ_t

We consider the following six cases: (C1) standard natural-shape balloon with 2.99% tendon slackness; (C2) standard natural-shape balloon with tendon/gore seam match; (C3) standard natural-shape balloon with 2.22% effective tendon shortening; (C4) pumpkin balloon, $r_B = 0.835$, and 2.99% tendon slackness; (C5) pumpkin balloon, $r_B = 0.835$, and tendon/gore seam match; and (C6) pumpkin balloon, $r_B = 0.835$, and 2.22% effective tendon shortening. Table 6 presents a summary of the numerical results related to cases C1–C6.

To illustrate the robustness of our approach, we used a sphere with a circumference equal to $2L_d$ as the initial configuration $\mathcal{S}^0$ (Fig. 4). Figure 4 includes profiles of the strained superpressure natural-shape balloon (C3) and strained pumpkin-shape balloon (C6). There were no convergence problems when computing a numerical solution

Table 6 Parametric Study C: Vary ϵ_t with $r_B = 0.78$ and $n_g = 290$; comparison of superpressure natural shape and pumpkin balloon

	Standard natural shape			Pumpkin shape		
Variable	Case C1	Case C2	Case C3	Case C4	Case C5	Case C6
Tendon slackness ϵ_t	0.0299	0.0	−0.0222	0.0299	0.0	−0.0222
Height, m	79.95	71.87	69.07	73.853	71.10	69.39
Diameter, m	113.83	114.17	112.58	119.86	116.81	114.344
Max δ_1, m/m	0.0338	0.0065	0.000	0.000	0.00	0.0000
Max δ_2, m/m	0.0358	0.0095	0.0128	0.0443	0.019	0.0097
Max $\bar{\sigma}_1$, MPa	78	15.34	0.00	28	3.91	0.00
Max $\bar{\sigma}_2$, MPa	78	15.42	5.25	40	10.10	4.25
Tendon tension range, kN	(2.0, 3.0)	(5.2, 4.3)	(4.6, 4.7)	(4.05, 5.10)	(4.7, 5.0)	(4.8, 4.9)

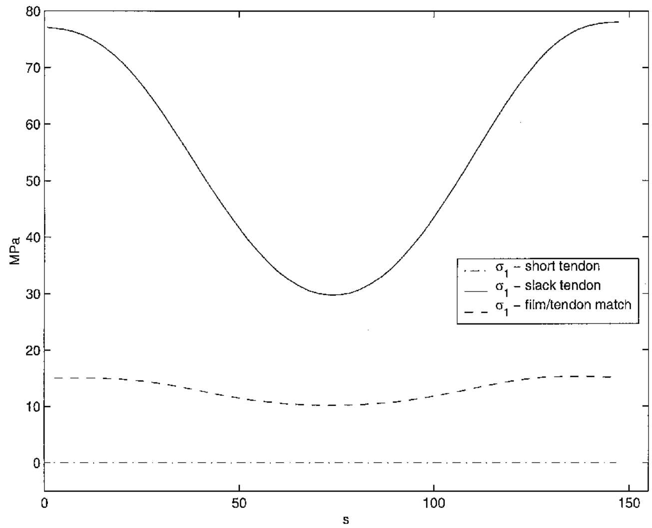

a) $\bar{\sigma}_1\,(s)$

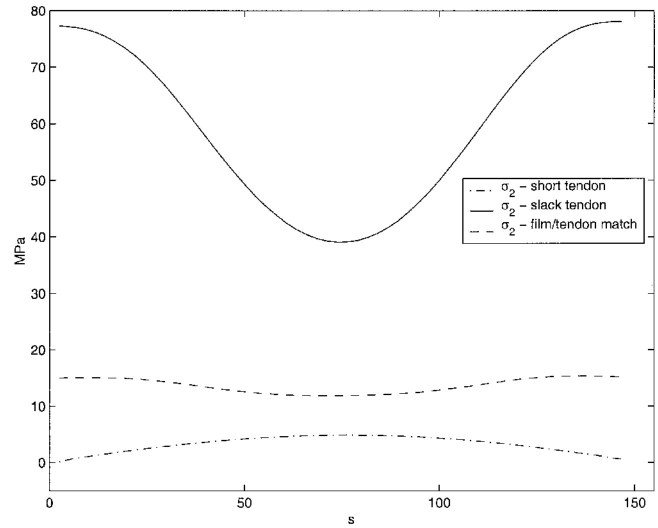

c) $\bar{\sigma}_2\,(s)$

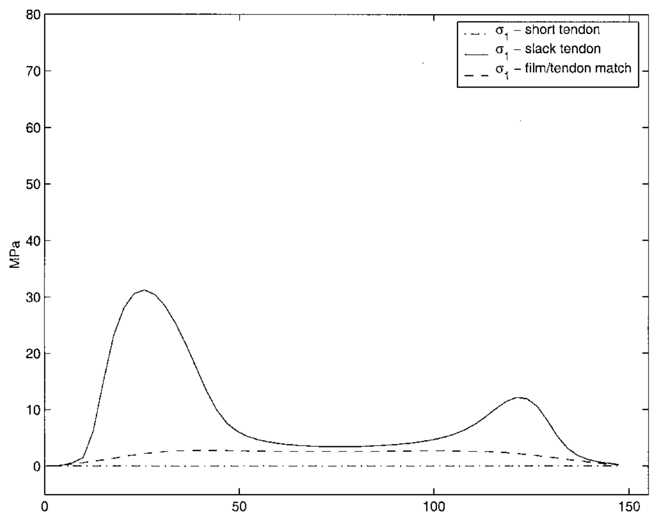

b) $\bar{\sigma}_1\,(s)$

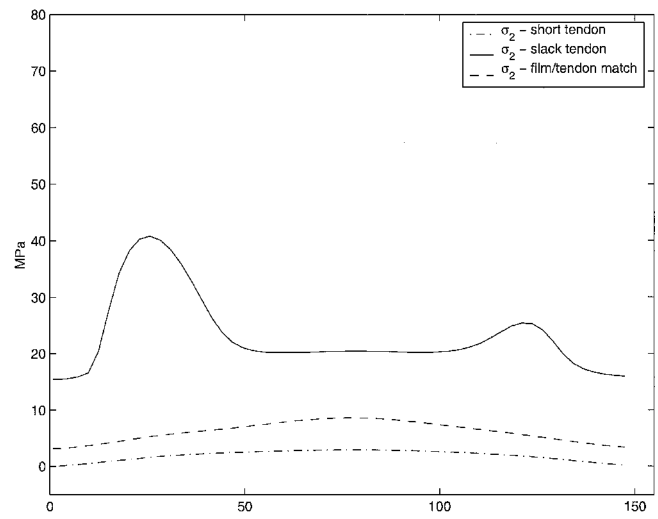

d) $\bar{\sigma}_2\,(s)$

Fig. 5 Parametric Study C averaged principal stresses of natural and pumpkin shapes.

of Problem ⋆. The pumpkin balloon is designed with the aim of reducing the film stresses by transferring most of the load into the tendons. Table 6 indicates the strained pumpkin balloon is doing exactly that.

In Fig. 5a we present plots of the averaged principal stress in a strained superpressure natural-shaped balloon (SPNS). The averaged principal stress in the film at a distance s from the bottom gore is denoted by $\bar{\sigma}_1(s)$. Three scenarios are considered: $\epsilon_t = -0.0222, 0.00, 0.0299$, corresponding to the cases of tendon shortening by 2.22%, 0% tendon slackness, and 2.99% tendon slackness, respectively. Similarly, Fig. 5c plots the averaged principal stress $\bar{\sigma}_2(s)$. Roughly speaking, $\bar{\sigma}_1(s)$ corresponds to the meridional direction, and $\bar{\sigma}_2(s)$ corresponds to the circumferential direction. Figure 5b contains a plot of the averaged principal stress $\bar{\sigma}_1(s)$ for the pumpkin balloon. Figure 5d contains a plot of the averaged principal stress $\bar{\sigma}_2(s)$ for the pumpkin balloon.

The data in Table 6 and the plots in Fig. 5 clearly demonstrate that film strength requirements are reduced by increasing the tendon stiffness, and tendon stiffness is increased by foreshortening the tendons.

The plots in Fig. 5 also illustrate that the shape of the pumpkin gore is more efficient than the standard natural-shape gore. Even with slack tendons, the maximum principal stresses in a pumpkin gore are roughly one-half the corresponding values in the natural-shape gore. For designs with gores that are in the unstrained state developable surfaces and for designs with gores that are bulged and wrinkled in the unstrained state, the unpublished detailed data for the parametric study presented in Ref. 4 show stress humps towards the gore ends similar to what is seen in Fig. 5. These humps diminish with increased tendon stiffness or tendon shortening as shown in Figs. 5b and 5d. In these designs a constant stress level is approached with very high tendon stiffness or with equivalent tendon shortening. For the designs analyzed in cases C3 and C6, Figs. 5a and 5b show that enough excess gore length relative to the tendon length is provided to guarantee meridional slackness of the entire gore under full load.

VI. Conclusions

The variational formulation in conjunction with optimization as a solution process offers definite advantages in certain situations over an implicit solution process in a finite element analysis of a membrane structure. A typical finite element method approach using an implicit solution process runs into difficulties when the stiffness matrix is noninvertible. Moreover, if numerous load increments are needed to reach the desired equilibrium state the computation time could be long. The optimization approach circumvents these difficulties by directly seeking a minimum unencumbered by the indefiniteness of unstable intermediate configurations in the evolution of the solution. The formulation exhibited here allows the modeling of wrinkled membranes (including the initial membrane state), and it allows the modeling of structural lack of fit between the gore and load tendon.

The analyses of the balloon designs in Parametric Studies C1–C6 demonstrate that designs in which tendons are shortened relative to the gore seam along which they track are superior to designs with slack tendons as are used in current zero-pressure balloons. In addition, they also demonstrate that further significant improvement is obtained by supplying excess gore width and gore length to promote circular arc bulging between tendons in the absence of meridional stresses in the gore. It is important to keep in mind that our methods are not dependent on the pumpkin balloon. The results on the pumpkin balloon that are presented here suggest the possibility of similar success if our methods are applied to more general pneumatic envelopes.

Acknowledgments

The first author was supported in part by NASA Grant NAG5-5292. We are grateful to the referees for their helpful comments.

References

[1]Smalley, J. H., "Development of the e-Balloon," National Center for Atmospheric Research, AFCRL-70-0543, Boulder, CO, June 1970.

[2]Rougeron, M., "Up to Date CNES Balloon Study," *Proceedings of the 10th Scientific Balloon Symposium*, AFGL-TR-79-0053, Portsmouth, NH, Aug. 1978.

[3]Yajima, N., "A New Design and Fabrication Approach for Pressurized Balloon," *Advances in Space Research*, Vol. 26, No. 9, 2000, pp. 1357–1360.

[4]Schur, W. W., "Analysis of Load Tape Constrained Pneumatic Envelopes," AIAA Paper 99-1526, April 1999.

[5]Baginski, F., and Collier, W., "Modeling the Shapes of Constrained Partially Inflated High-Altitude Balloons," *AIAA Journal*, Vol. 39, No. 9, 2001, pp. 1662–1672; "Errata," *AIAA Journal*, Vol. 40, No. 6, 2002, p. 1253.

[6]Baginski, F., and Brakke, K. A., "Modeling Ascent Configurations of Strained High-Altitude Balloons," *AIAA Journal*, Vol. 36, No. 10, 1998, pp. 1901–1910.

[7]Collier, W., "Applications of Variational Principles to Modeling a Partially Inflated Scientific Research Balloon," Ph.D. Dissertation, Dept. of Mathematics, George Washington Univ., Washington, DC, Jan. 2000.

[8]Pipkin, A. C., "Relaxed Energy Densities for Large Deformations of Membranes," *Journal of Applied Mathematics*, Vol. 52, 1994, pp. 297–308.

[9]Morris, A. L. (ed.), "Scientific Ballooning Handbook," National Center for Atmospheric Research, NCAR-TN-99, Boulder, CO, May 1975.

[10]do Carmo, M. P., *Differential Geometry of Curves and Surfaces*, Prentice–Hall, Upper Saddle River, NJ, 1976, p. 89.

[11]Ciarlet, P. G., *Mathematical Elasticity Volume III: Theory of Shells*, North-Holland, New York, 2000, pp. 335–344.

A. Messac
Associate Editor